Chinese Chemical Letters 36 (2025) 109898

Contents lists available at ScienceDirect

Chinese Chemical Letters

journal homepage: www.elsevier.com/locate/cclet

# The advanced development of one-dimensional transition metal dichalcogenide nanotubes: From preparation to application

Fengshun Wang[a], Huachao Ji[a], Zefei Wu[a], Kang Chen[a], Wenqi Gao[b], Chen Wang[b], Longlu Wang[a,*], Jianmei Chen[a], Dafeng Yan[b,*]

[a] College of Electronic and Optical Engineering & College of Flexible Electronics (Future Technology), Nanjing University of Posts & Telecommunications (NJUPT), Nanjing 210023, China
[b] Hubei Key Laboratory for Precision Synthesis of Small Molecule Pharmaceuticals & Ministry of Education Key Laboratory for the Synthesis and Application of Organic Functional Molecules & College of Chemistry and Chemical Engineering, Hubei University, Wuhan 430062, China

ARTICLE INFO

*Article history:*
Received 29 February 2024
Revised 27 March 2024
Accepted 16 April 2024
Available online 16 April 2024

*Keywords:*
One-dimensional transition metal sulfides
Nanotubes
Structure
Preparation method
Applications

ABSTRACT

Two-dimensional (2D) transition metal sulfides (TMDs) are emerging and highly well received 2D materials, which are considered as an ideal 2D platform for studying various electronic properties and potential applications due to their chemical diversity. Converting 2D TMDs into one-dimensional (1D) TMDs nanotubes can not only retain some advantages of 2D nanosheets but also providing a unique direction to explore the novel properties of TMDs materials in the 1D limit. However, the controllable preparation of high-quality nanotubes remains a major challenge. It is very necessary to review the advanced development of one-dimensional transition metal dichalcogenide nanotubes from preparation to application. Here, we first summarize a series of bottom-up synthesis methods of 1D TMDs, such as template growth and metal catalyzed method. Then, top-down synthesis methods are summarized, which included self-curing and stacking of TMDs nanosheets. In addition, we discuss some key applications that utilize the properties of 1D-TMDs nanotubes in the areas of catalyst preparation, energy storage, and electronic devices. Last but not least, we prospect the preparation methods of high-quality 1D-TMDs nanotubes, which will lay a foundation for the synthesis of high-performance optoelectronic devices, catalysts, and energy storage components



## 1. Introduction

Two-dimensional (2D) transition metal sulfides (TMDs) are considered ideal 2D platforms for exploring various electronic properties and potential applications due to their unique physical and chemical properties [1–5]. Single or multilayer 2D-TMDs materials typically exhibit excellent electronic, optical, and structural properties, and thus have been subjected to a wide range of theoretical and experimental research in the field of electronics and energy [6–10]. Interestingly, the conversion of the 2D-TMDs material into one-dimensional (1D) nanotubes can not only retain some of the advantages of 2D nanosheets, but also exhibit exceptional flexibility, tunable electronic properties, and other novel properties based on their chirality and composition structure [11–17]. However, the controllable preparation of single or multiple layers of high-quality nanotubes remains challenging [18–26]. On the one hand, it is difficult to precisely control the inner diameter of single-walled and multi-walled nanotubes during the preparation process [27–36]. On the other hand, the number of layers in the wall is also difficult to control during the preparation of multi-walled nanotubes [37–44].

Different methods have been developed for the preparation of nanotubes, such as template method, metal catalysis method, curling method, stacking method. Due to the high stability, uniformity, and removability of anodized aluminum oxide (AAO), it has been widely used as template to prepare nanotubes. Liu *et al.* [45] prepared $MoS_2$ nanotubes with controllable diameters on AAO templates by atomic layer deposition (ALD) technique. Yusuke *et al.* [46] used boron nitride nanotubes ($BNNT_S$) as a coaxial growth template of nanotubes, then prepared BN@$MoS_2$NTs and $MoS_2$@BNNTs in the inner lumen and on the outer surface of the templates, respectively. In fact, the inner diameter of 1D-TMDs nanotubes can be precisely adjusted based on a template sacrifice strategy.

* Corresponding authors.
*E-mail addresses:* wanglonglu@hnu.edu.cn (L. Wang), dafengyan@hubu.edu.cn (D. Yan).

https://doi.org/10.1016/j.cclet.2024.109898
1001-8417/

Xu *et al*. [47] used stable nanowires (NWs) with simple synthesis as the inner core growth template of nanotubes, and synthesized hollow $WS_2$, $WSe_2$ and $WS_{2(1-x)}Se_{2x}$ nanotubes with controllable components by chemical vapor method. In addition, multilayer inner wall nanotubes can be prepared by self-curing and stacking of flexible nanosheets. Suh *et al*. [48] prepared nanotubes with coil structure by adding self-assembly material to the stripped 2H-$MoS_2$ nanosheets. Jia *et al*. [49] synthesized nanotubes with N-doped-C layer-stacked structures based on solvent-thermal method by using flexible and deformable nanosheets. Deepak *et al*. [37] believe that research in this field still holds great potential in the coming years as new synthesis methods and new structures for nanotubes become available. Therefore, it is much necessary to summarize the preparation methods of high-quality 1D-TMDs nanotubes, which can guide more researchers focus on this hot topic and promote the development of the1D-TMDs.

In this paper, we review the preparation methods of high-quality 1D-TMDs nanotubes from two perspectives. On the one hand, we summarized the specific synthesis methods of nanotubes from the bottom-up perspective, such as template method and metal-catalyzed method [50–56]. On the other hand, based on the top-down perspective, we summarize the methods of preparing nanotubes by self-curing and stacking flexible nanosheets [57–59]. Finally, we emphasize the importance of preparing high-quality 1D-TMDs nanotubes for the study of their interesting and potential properties and applications.

## 2. Bottom-up preparation

The bottom-up preparation method is to form a relatively complex structural system with definite shape, size and chemical composition through the growth and self-assembly of atoms and molecules with smaller structural units. This method is based on the self-assembly of atoms and molecules and other means and fabrication techniques, from the gas phase or liquid phase to the solid phase of the chemical process, such as vapor deposition, liquid phase deposition, hydrothermal solvent method [60–63]. The bottom-up approach allows for regulated growth at the nanoscale or even atomic and molecular scales using various templates as the basic units of multilevel structures, enabling the construction of three-dimensional structures as needed in three spatial dimensions, thus making more efficient use of raw materials.

### *2.1. Template method*

Template method is considered to be the most widely used method for preparing nanomaterials with special morphology and structure. The template method is to deposit related atoms or ions into the holes or surfaces of the pre-prepared rigid templates by physical and chemical methods, and then sacrifice the templates to obtain the required nanostructured materials [64]. According to the different morphology and structure, the rigid template includes carbon nanotubes, honeycomb template, NWs, and so on.

#### *2.1.1. Based on AAO template*

The anodized aluminum oxide (AAO) with high stability, uniformity and removability, is very suitable for the preparation of ordered nanotube arrays. The sacrificial strategy of AAO template enabled preparation of nanotubes with controllable wall thickness and diameter [65].

Liu *et al*. [45] prepared $MoS_2$ nanotubes arrays ($MoS_2$_NTA) on $Ti_3C_2$ substrate by ALD technique based on AAO honeycomb template method (Fig. 1a). The diameter and wall thickness of $MoS_2$_NTA could be controlled by adjusting the cellular diameter of the AAO template and the number of ALD cycles, respectively. Fig. 1b showed the upper face and cross section of the AAO honeycomb template, indicating the integrity of the channel and the smoothness of the surface. The $MoS_2$/AAO/$Ti_3C_2$ film was placed in 20 mL 5 mol/L NaOH solution for 12 h to remove the AAO template successfully. As shown in Fig. 1c, continuous and complete $MoS_2$_NTA were presented on the substrate, indicating that $MoS_2$_NTA had been successfully prepared.

Based on the AAO honeycomb template sacrifice strategy, Han *et al*. [66] prepared graphene nanotube frames by restricted assembly of $Fe_3O_4$ nanocrystals and graphitization of tubular carbon frames (Fig. 1d). AAO templates with uniform and regular channel arrays provided a stable environment for the self-assembly of $Fe_3O_4$ nanocrystals to form nanotubes inside the channels in an epitaxial growth-like manner. Etching with KOH (6 mol/L) for 6 h could easily remove the AAO template and obtain an ordered $MoS_2$_NTA. As shown in Fig. 1e, there were ordered mesoporous pores on a single graphene NT, the pore size could be adjusted by changing the size of the $Fe_3O_4$ nanocrystals used for self-assembly. Fig. 1f showed $MoS_2$@C van der Waals super-tubes prepared by confining the epitaxial growth of arc-shaped $MoS_2$ with few layers to a tubular mesoporous graphene framework. Fig. 1g showed small-angle X-ray scattering (SAXS) pattern of $MoS_2$@C super-tube and tubular graphene frameworks. $MoS_2$@C super-tube showed multiple clear peaks resulting from ordered mesoporous properties confirming its multi-mesoporous structure.

Liang *et al*. [67] prepared ordered and homogeneous 1D $MoS_2$ nanotubes ($MoS_2$_ONT) by uniformly depositing $MoS_2$ inside a porous AAO honeycomb template based on chemical vapor deposition (CVD) using S powder as the sulfur source and $MoO_3$ as the molybdenum source (Fig. 1h). As shown in Figs. 1i and j, the $MoS_2$_ONT obtained by soaking $MoS_2$_ONT/AAO in 1 mol/L NaOH solution for 72 h to remove the AAO template exist in an array structure, forming tubular confined spaces. The semi-transparent black color rendered by $MoS_2$_ONT indicated that $MoS_2$_ONT had excellent light absorption capacity, which was important for its application in the field of photocatalysis (illustration in Fig. 1j). Fig. 1k showed the Raman spectra, confirming that $MoS_2$_ONT had better crystallinity and better spatial scalability, which enabled it to exhibit better light absorption properties and faster electron transfer. This method of preparing nanotubes based on AAO honeycomb template sacrifice strategy could be extended to the synthesis of other TMDs nanotubes with stable, controllable morphology and novel characteristics.

#### *2.1.2. Based on one-dimensional material template*

The tubular inner cavities and outer surface of the template could be used as a template for the coaxial growth of exotic nanotubes, and single-walled TMDs nanotubes with different diameters could be prepared by adjusting the size of the template's inner and outer diameters [68]. The nanotubes with several nanometers wide could be stabilized by a protective template with the same geometry for their characterization.

Yusuke *et al*. [46] studied the vapor-phase growth of single-walled $MoS_2$ nanotubes with various diameters. As shown in Fig. 2a, BN@$MoS_2$NTs and $MoS_2$@BNNTs were prepared based on the outer and inner walls of the BNNTs template, respectively. Based on the growth positions, the nanotubes had different diameters. Figs. 2b and c showed the HAADF-STEM images of BN@$MoS_2$NTs and $MoS_2$@BNNTs. The results indicated that the outer $MoS_2$ wall of BN@$MoS_2$NTs was much brighter than the inner BNNT core, while the inner wall center part of $MoS_2$@BNNTs was brighter. EELS chemistries of BN@$MoS_2$NTs and $MoS_2$@BNNTs (Figs. 2b and c) showed the specific distribution of Mo and S elements on the outermost layer and inner walls of BNNTs, confirming two distinct coating structures. In addition, $MoS_2$@BNNTs protected the ultrathin $MoS_2$ nanotubes from electron beam damage and oxidation due to the protection of the external BNNTs template. Therefore,

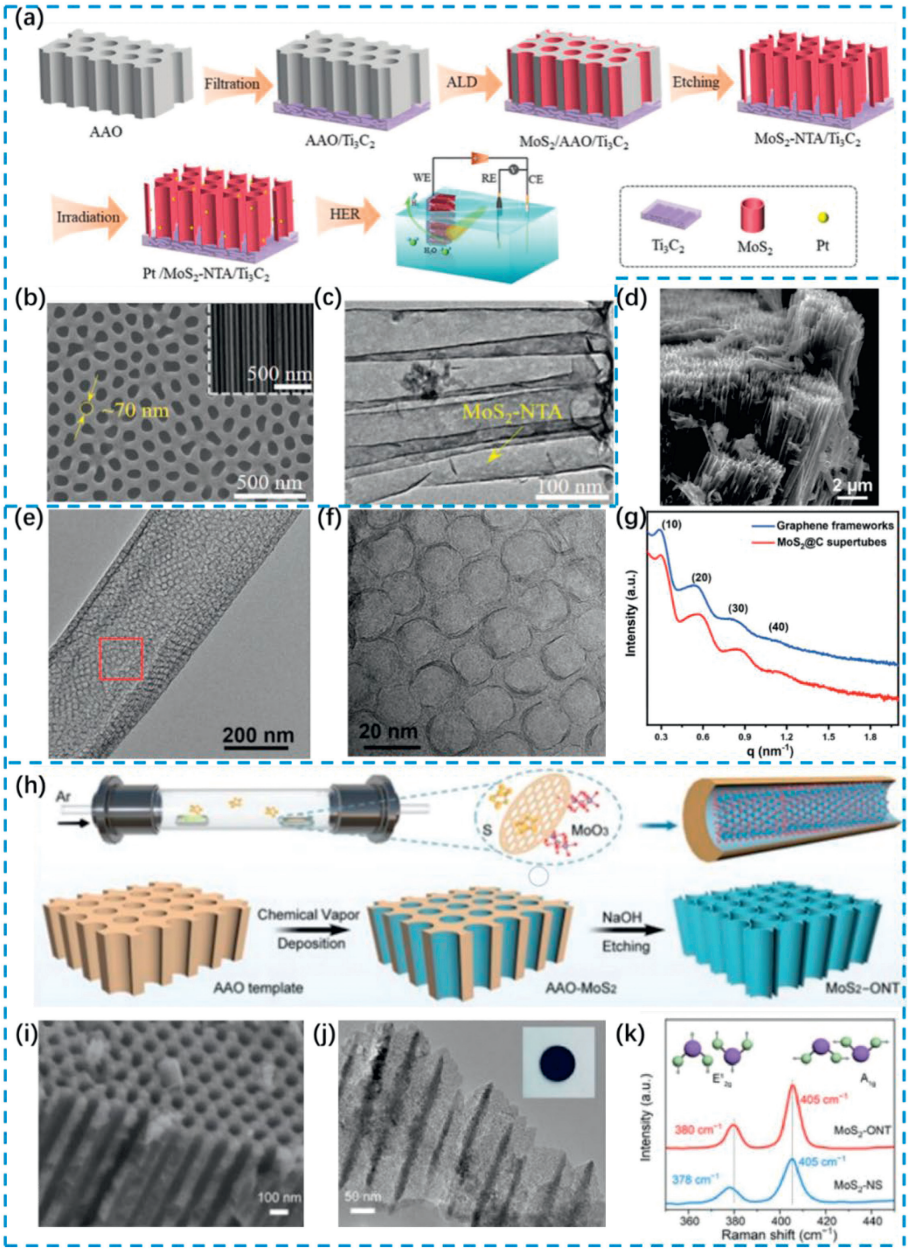


**Fig. 1.** (a) Experimental flowchart for the synthesis processes of Pt/$MoS_2$-NTA/$Ti_3C_2$. (b) the upper surface and cross-section (the inset) of AAO. (c) TEM image of $MoS_2$-NTA in $MoS_2$-NTA/$Ti_3C_2$. Reproduced with permission [45]. Copyright 2022, Wiley-VCH GmbH. (d) Low-magnification SEM images of tubular graphene frameworks existing as 1D arrays. (e) TEM image of a single $MoS_2$@C supertubes. (f) HRTEM image of the region indicated by the square in (e). (g) SAXS patterns of $MoS_2$@C supertubes and tubular graphene frameworks. Reproduced with permission [66]. Copyright 2023, Wiley-VCH GmbH. (h) Schematic diagram of preparing $MoS_2$-ONT by template method. (i) SEM and (j) TEM images of $MoS_2$-ONT. Inset: The optical photo of $MoS_2$-ONT. (k) Raman spectra of $MoS_2$-ONT and $MoS_2$-NS. Reproduced with permission [67]. Copyright 2023, Wiley-VCH GmbH.

the inner cavities of BNNTs allowed the preparation of ultrathin $MoS_2$ nanotubes with diameters below 5 nm (Fig. 2d), which was critical to facilitate further preparation and research of single-wall TMD nanotubes. The BNNT template reaction provided a versatile platform that could be applied to further prepare various TMD nanotubes with better performance.

Chen *et al.* [69] synthesized ultrasmall monolayer $NbSe_2$ flat nanotubes with equivalent circular diameters (<2.31 nm) based on the chemical reaction inside carbon nanotubes (CNTs) for self-pressurization and the deselenization reaction of internally encapsulated $NbSe_3$ chains. As shown in Figs. 2e and f, $NbSe_2$ nanotubes inside CNT had obvious elliptic characteristics. Due to the differences in different stacking methods of the upper and lower walls of the $NbSe_2$ nanotubes, the nanotube interiors showed two different honeycomb structures (Figs. 2g and h). Fig. 2i showed the Raman spectra of $NbSe_2$@CNT obtained under different laser wavelengths. The upward shift of the $NbSe_2$@CNT characteristic peak proved that CNT is compressed during the formation of $NbSe_2$ nanotubes, and that strain was introduced into CNT. This method of nanotubes prepared based on tubular templates provides a pioneering idea for the preparation of high-quality nanotubes.

NWs were structurally stable and simple to be synthesized on a large scale on various substrates [70]. Therefore, using the NWs template to prepare hollow nanotubes could not only effectively improve the structural stability of nanotubes, but also save the preparation cost. In addition, since the nanotubes and NWs were

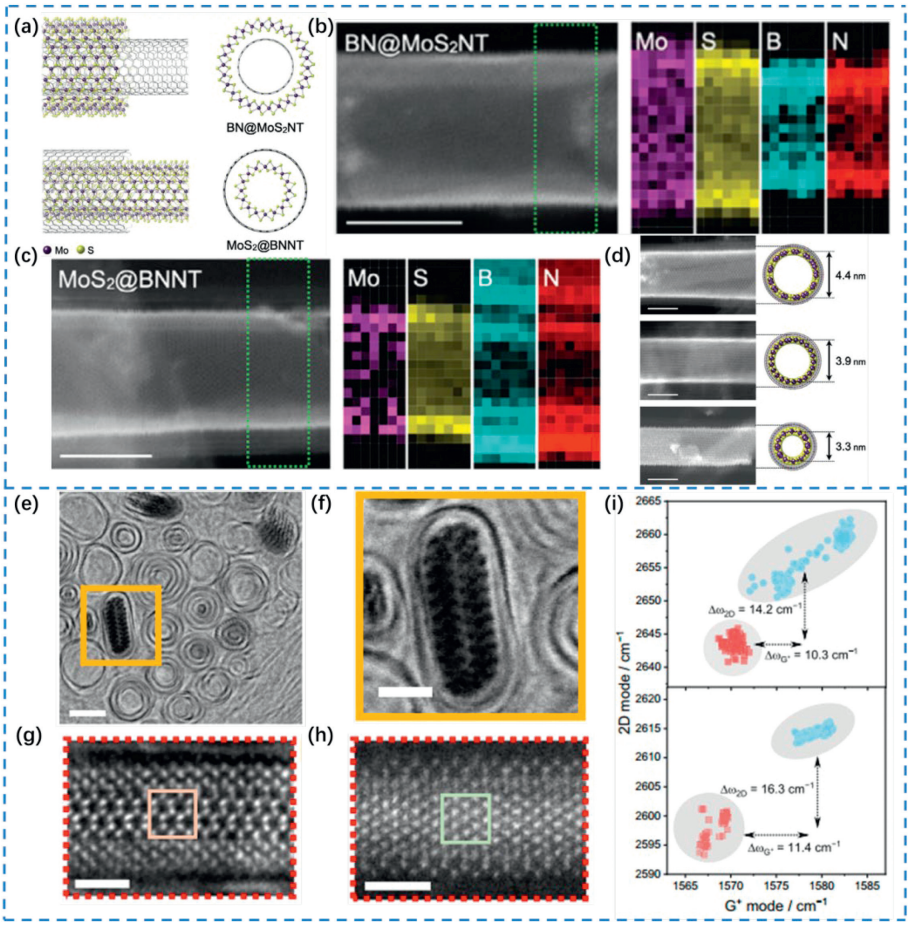


**Fig. 2.** (a) Schematic illustration of the atomic structure of a single-walled $MoS_2$ nanotubes that grows coaxially inside and outside the BNNT template. (b) HAADF-STEM, and (c) EELS chemical maps of the BN@$MoS_2$NT and $MoS_2$@BNNT, respectively. Scale bars: 5 nm. (d) $MoS_2$ nanotubes with different tube diameters are confined to BNNT. Scale bars: 3 nm. Reproduced with permission [46]. Copyright 2023, Wiley-VCH GmbH. (e) Atomic-resolved cross-sectional BF images of single-layered flattened $NbSe_2$ nanotubes. (f) Enlarged image of the yellow box area in (e). (g) ADF image of $NbSe_2$ flat tube in AB-stack mode and (h) AA-stacked $NbSe_2$ flat tube with filled honeycomb structure. (i) Raman mode scatter plots of samples at 532 nm (up) and 633 nm (down) laser excitation wavelengths and correlation of 2D band positions with G-band positions. Primitive CNTs and $NbSe_2$@CNT flat heterogeneous tubes were marked with red squares and blue circles, respectively. Reproduced with permission [69]. Copyright 2024, Springer Nature.

grown coaxially, the diameter and length of the nanotubes could be directly controlled by adjusting the diameter and length of the NWs [71–73].

Xu *et al.* [47] synthesized $WS_2$, $WSe_2$ and component-controllable $WS_{2(1-x)}Se_{2x}$NT on flexible carbon fiber (CF) by chemical vapor method. Fig. 3a showed the synthesis process of $WS_2$NT. The $WO_3$ NWs grown on CF served as a conversion template, and $WS_2$NT was prepared by sulfurization. Using the same method, $WSe_2$NT was also prepared by subjecting $WO_3$ NWs to selenization. By varying the ratio of S and Se precursors, the group controllably synthesized serial ternary $WS_{2(1-x)}Se_{2x}$NT. Gao *et al.* [74] prepared $MoS_2$@$CoS_2$ heterojunction hollow nanotubes with double-layer structures by combining simple electrospinning, pyrolysis and vulcanization processes (Fig. 3b). Fig. 3c showed the TEM images of $MoO_3$@$Co_3O_4$ nanofibers, which confirmed that it possessed a bilayer hollow structure. $MoO_3$@$Co_3O_4$ was vulcanized in $N_2$ atmosphere and transformed into $MoS_2$@$CoS_2$, while it still possessed an obvious double-walled hollow structure (Fig. 3d). Fig. 3e showed the XRD pattern of $MoS_2$@$CoS_2$, confirming the successful preparation of the heterogeneous composition of $MoS_2$@$CoS_2$. Wei *et al.* [75] synthesized $Cu_2S$/$Cu_2O$ heterojunction nanotubes on Cu NWs by a simple hydrothermal method. As shown in Fig. 3f, the prepared Cu/$Cu_2O$ NWs had a smooth surface and straight shape. After the vulcanization process, the Cu/$Cu_2O$ NWs was transformed into Cu/$Cu_2O$/$Cu_2S$NT (Fig. 3g), which presented a hollow structure and a rough surface. Fig. 3h showed the XRD patterns of the prepared NWs and NT, confirming the successful synthesis of Cu/$Cu_2O$/ $Cu_2S$ NT from the NWs prepared by vulcanization. The method of preparing nanotubes based on NWs templates not only controlled the structure of the nanotubes, but also allowed for the preparation of multi-walled layered nanotubes. This method provided a reference for the preparation of stable structure of layered nanotubes.

### 2.2. Metal catalyzed method

By using nanoparticles (NPs) as the accommodating sites for the growth of TMDs, high-quality TMD nanotubes could be directly and controllably prepared based on the CVD method. Meanwhile, the growth of TMD nanotubes could be controlled by precisely adjusting the temperature of the reaction process.

An *et al.* [76] directly prepared $WS_2$ nanotubes with controllable chirality using Au NPs as catalyst based on CVD method (Fig. 4a). Fig. 4b (Steps 1–4) showed a comparison between the direct growth of TMDs nanocrystals on Si substrate and the using of Au NPs as catalyst, indicating that the presence of Au NPs could serve as accommodative sites for $WO_3$ and S/Se vapors. Meanwhile, $WO_3$ crystalline layer could be formed on the surface of Au NPs, and

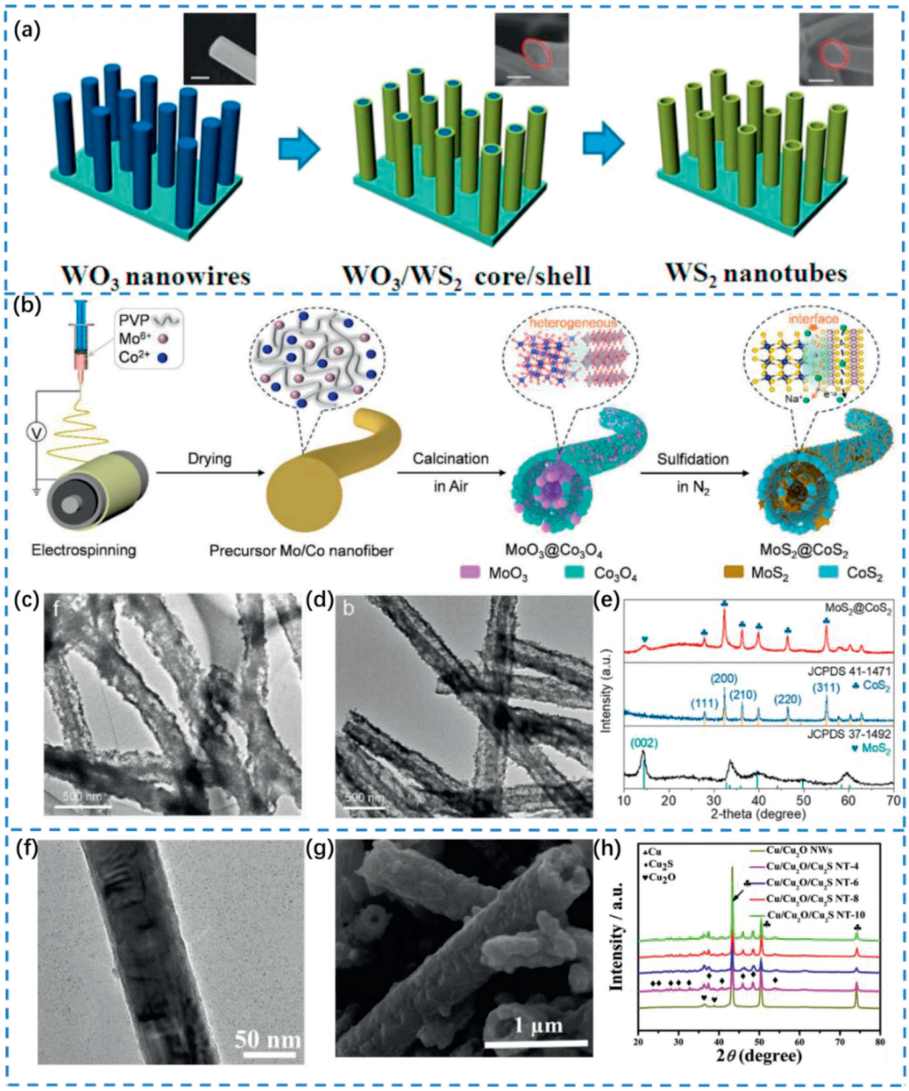


**Fig. 3.** (a) Growth process of $WO_3$ NWs converting to $WS_2$, $WSe_2$, and $WS_{2(1-x)}Se_{2x}$ nanotubes on CFs by sulfuration and selenization. Reproduced with permission [47]. Copyright 2014, American Chemical Society. HRTEM image of (b) schematic diagram of preparing $MoS_2$@$CoS_2$ heterostructure tube-in-tube hollow nanofibers. (c, d) TEM images of $MoO_3$@$Co_3O_4$ and $MoS_2$@$CoS_2$ tube-in-tube nanofibers. (e) XRD pattern of $MoS_2$@$CoS_2$ tube-in-tube nanofibers. Reproduced with permission [74]. Copyright 2024, Elsevier B.V. (f) TEM of as-prepared Cu/$Cu_2O$ NWs. (g) FESEM images of as-prepared Cu/$Cu_2O$/$Cu_2S$ NT. (h) XRD patterns of Cu/$Cu_2O$ NWs, and Cu/$Cu_2O$/$Cu_2S$ NT for 4, 6, 8, 10 h. Reproduced with permission [75]. Copyright 2019, Elsevier B.V.

then converted into TMD monolayer. Adjusting the temperature during the reaction process can impact the morphology and nucleation sites of nanotubes, which means that nanotubes exhibit different growth modes at different temperatures. Fig. 4b (Steps 5 and 6) showed the different growth patterns of single chiral angle and multiple chiral angle nanotubes at different controlled temperatures. This particular growth mechanism is quite different compared to the method based on $WO_{3-x}$ NWs as a template for the sulfurization synthesis of $WS_2$ nanotubes. At the growth temperature of ~835–840 °C, the nucleation sites of $WS_2$ nanotubes were located at the edge contact between Au nanoparticles and the Si substrate. The growth of nanotubes is mainly determined by edge energetics. Further growth and extension of the $WS_2$ lamellae led to an increase in the internal strain within the layers thereby spontaneously curling to form $WS_2$ nanoscrolls with single or multiple walls. The nanoscrolls-based infrastructure was further grown layer by layer to form a multi-walled $WS_2$ nanotube (Fig. 4d). At the growth temperature of ~840–845 °C, the nucleation sites of $WS_2$ nanotubes were located on the surface of Au nanoparticles, and the nanotubes primarily grew *via* surface growth mode (Fig. 4c). The $WS_2$ shells on the surface of the NPs form a polyhedral faceting through continuous epitaxial layer by layer growth, and form multi-walled seamless nanotubes with different helicity based on the simultaneous extensive growth along the tangential and perimeter angles.

The method of preparing nanotubes based on metal catalyzed method lifts the dependence on template and has wide applicability. At the same time, this method of synthesizing controllable chiral angular TMD nanotubes greatly expands the possibility of studying their physical properties and practical applications.

## 3. Top-down preparation

The top-down preparation method uses mechanical, chemical, or other forms of energy to transfer the bulk material into nanotubes of the desired structure. There are mainly two methods of top-down preparation have been reported to transfer the TMDs nanosheets into nanotubes. On the one hand, large nanosheet layers could be transformed into nanotubes by utilizing the curling effect of them; on the other hand, small nanosheet layers could be

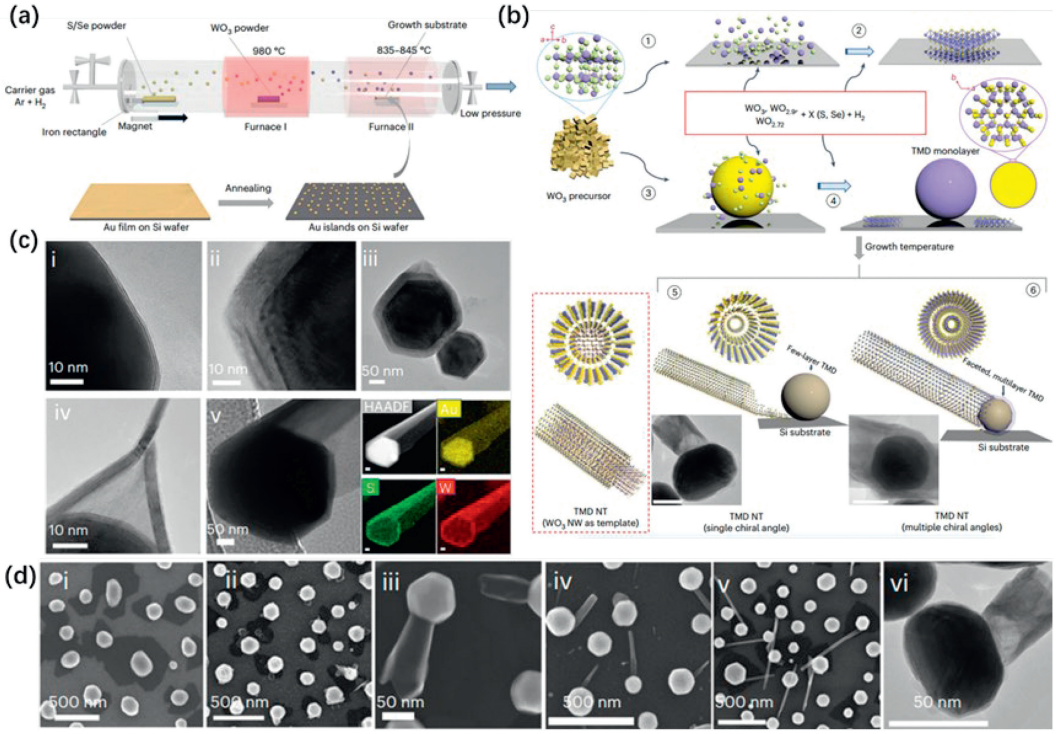


**Fig. 4.** (a) Preparation of Au NPs catalyst and CVD growth of TMD nanotubes. (b) The growth mechanism of TMD nanotubes, shown in the dashed line box, is a schematic diagram of metal oxide NWs vulcanization to prepare TMDs nanotubes. (c) TEM images of the growth of $WS_2$ nanotubes at ~840–845 °C. The EDS map is in the bottom right corner. HAADF, high Angle ADF. (d) SEM images of the growth process of $WS_2$ nanotubes at ~835–840 °C. Reproduced with permission [76]. Copyright 2023, Springer Nature.

stacked into nanotube-like structures by the stacking effect. In the following parts, we will introduce the top-down method of preparing nanotubes from these two aspects [60,61].

### 3.1. Fabrication of nanotubes derived from the curled nanosheets

The flexible two-dimensional nanosheets could be assembled into nanotubes with layered structures by drying, dropping solvent and freezing [77,78]. Amount of stress applied to the surface of the nanosheets could be controlled by adjusting the time of the reaction, thereby tuning the structure of the nanotubes [48,79–81].

Ghosh *et al.* [82] synthesized $WS_2/MoS_2$ heterogeneous films on $Si/SiO_2$ substrate by CVD method. Based on the flexibility of the nanofilm and its weak interaction with the substrate, $WS_2/MoS_2$ nanoscrolls with tubular structure were prepared by rolling the nanofilms with evaporation assistance (Fig. 5a). Liu *et al.* [83] mixed the stripped $Ti_3C_2T_X$ nanosheets with ammonium tetrathiopolybdate (ATM), and used liquid nitrogen to rapidly freeze dry them to shrink and automatically curl to form tubular NS. The dried $ATM/Ti_3C_2T_X$ mixture was further annealed in $H_2/Ar$ atmosphere to obtain the final $MoS_2/Ti_3C_2T_X$ tubular NS (Fig. 5b). Jiang *et al.* [84] used laser molecular beam epitaxy (LMBE) technology to confine the single atoms (SAs) of Ni and Fe to two adjacent layers of $MoS_2$ and, through subsequent self-bending treatment, prepared $NiFe@MoS_2$ tubular NS (Fig. 5c). $NiFe@MoS_2$ NS possessed obvious tubular and layered structures, which provided a suitable microenvironment for limiting Ni and Fe SAs. Kato *et al.* [85] grew Janus WSSe and MoSSe monolayers based on plasma-assisted surface atom substitution, and prepared Janus nanoscrolls by dropping a solution to make them self-curl. As shown in Figs. 5d and e, monolayer $MoSe_2$ and $WSe_2$ single crystals were prepared on $SiO_2/Si$ substrate based on CVD method. Double-sided WSSe and MoSSe monolayers were prepared by replacing Se atoms with S atoms on the surface of one side of the $MoSe_2$ monolayer by means of plasma treatment (Figs. 5f and g). Finally, the substrate was spin-coated with a polymethyl methacrylate (PMMA)/chloroform solution, which caused the single-layer Janus film to spontaneously curl into Janus nanoscrolls (Figs. 5h and i). The method of preparing tubular NS based on the flexibility of nanosheets is simple and easy to operate, which is of great significance for the preparation of nanotubes.

### 3.2. Fabrication of nanotubes derived from stacked nanosheets

Based on interlayer stacking method, flexible $MoS_2$ nanosheets could controllably prepare nanotubes with interlayer expansion [86–91]. After further thermal treatment, the nanotubes were formed by alternating hybridization of $MoS_2$ nanosheets and C layers [92–97].

Jia *et al.* [49] synthesized $MoS_2$/OAm tubes with layer stacked structure based on solvothermal method using $MoO_3$ as molybdenum source, S powder as sulfur source, oleylamine (OAm) as a key additive and ethanol-water solution as a mixed solvent. The OAm existed in the gap between $MoS_2$ layers as an intercalation, while encapsulated single-layer $MoS_2$ as an encapsulating agent. The $MoS_2$/OAm tube was converted to a $MoS_2$/N-doped-C tube by further thermal treatment (Fig. 6a). As shown in Figs. 6b and c, TEM images confirmed that the $MoS_2$/N-doped C tube surface was formed by alternating stacking of multilayer $MoS_2$ nanosheets and N-doped C layers. Fig. 6d showed the XRD pattern of the prepared $MoS_2$/N-doped-C tube, which confirmed that the spacing of $MoS_2$ layers increased due to the alternating stacking of the N-doped-C layer and the $MoS_2$ nanosheets.

The nanotubes stacked by octylamine-covered layered nanosheets were synthesized based on a solvothermal method using octylamine as a key additive by Shi *et al.* [98]. The $MoS_2$:C superstructure nanotubes (Fig. 6e) were prepared by further thermal treatment of the nanotubes. As shown in Fig. 6f, the $MoS_2$:C

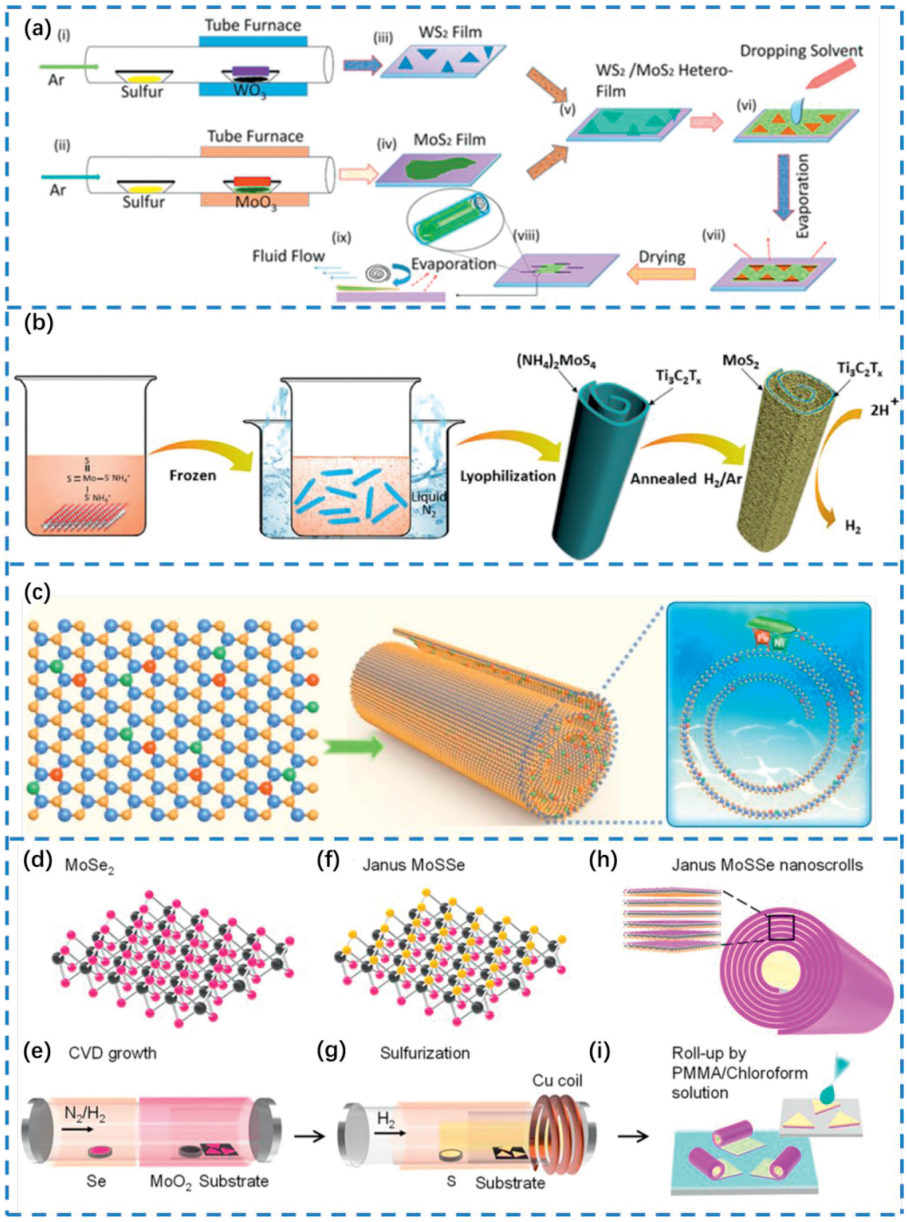


**Fig. 5.** (a) Schematic diagram of steps for preparing $WS_2/MoS_2$ heterojunction nanoscroll (NS). Reproduced with permission [82]. Copyright 2022, American Chemical Society. (b) The "nanoroll" $MoS_2/Ti_3C_2T_x$ hybrid material was prepared by the method of liquid nitrogen-freezing and subsequent annealing. Reproduced with permission [83]. Copyright 2018, Elsevier B.V. (c) The diagram of precisely assembling dual (Das) within in two adjacent layers in a nanoscroll structure. Reproduced with permission [84]. Copyright 2023, John Wiley & Sons, Inc. (d) Structure model of monolayer $MoSe_2$. (e) The process diagram of preparing monolayer layer $MoSe_2$ on $SiO_2/Si$ substrate with $MoO_2$ and Se as raw materials at 870 °C. (f) Structure model of Janus monolayer MoSSe. (g) Diagram of hydrogen plasma-assisted sulfurization process. (h) Structure model of Janus MoSSe nanoscrolls. (i) Rolling up process of Janus monolayers by spincoating of a PMMA/chloroform solution. Reproduced with permission [85]. Copyright 2024, American Chemical Society.

superstructure nanotubes have a layered stacked surface and a hollow structure. Fig. 6g showed TEM image of the $MoS_2$:C superstructure nanotubes, confirming that the nanotube surface was composed of multiple layers of tiny nanosheets stacked together. Meanwhile, Fig. 6g also showed that the lattice fringe spacing is 0.98 nm, indicating that the interlayer distance of the nanosheets in the C-layer embedded nanotubes was significantly increased. XRD patterns of the prepared and annealed nanotubes confirmed that the nanolayer spacing in $MoS_2$:C superstructure nanotubes was greatly increased (Fig. 6h). The increase of the peak strength of the sample after annealing indicated that the crystallinity of the sample was also enhanced. Based on the flexible $MoS_2$ nanosheets, the structure growth of composite nanotubes was effectively controlled by alternating stacking with the introduced C-layer. The ordered three-dimensional structure and suitable spatial configuration enabled the nanotubes to show some new characteristics.

## 4. Application of TMDs nanotube

1D-TMDs nanotubes are widely used in electronics and energy fields due to their unique physical and chemical properties. High-quality 1D-TMDs nanotubes can be used to prepare catalysts, energy storage batteries, photodetectors and superconductivity with excellent performance [99–102].

Electrochemical water splitting, as a promising method for hydrogen production, is considered a possible solution to the energy shortage issue due to its wide sources, high energy density, and

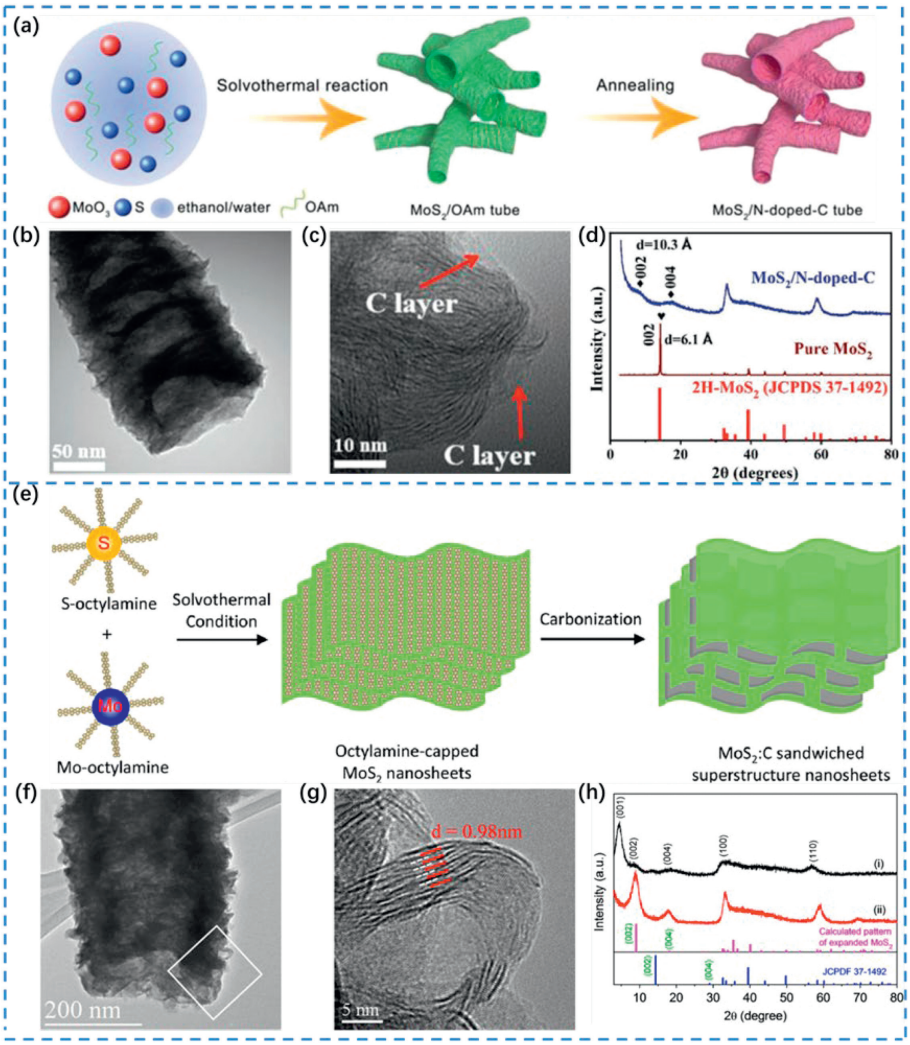


**Fig. 6.** (a) Synthesis process of the porous $MoS_2$/N-doped-C nanotube. (b, c) TEM and HRTEM image of the porous $MoS_2$/N-doped-C nanotube. (d) XRD patterns of pure $MoS_2$ and $MoS_2$/N-doped-C nanotubes. Reproduced with permission [49]. Copyright 2018, Wiley-VCH Verlag GmbH & Co. KGaA, Weinheim. (e) Schematic diagram of the preparation process of $MoS_2$:C superstructure nanosheets. (f) TEM and (g) HRTEM images of the $MoS_2$:C superstructure nanotubes after post thermal treatment. (h) XRD patterns of (i) the as-prepared $MoS_2$:C nanotubes and (ii) the annealed $MoS_2$:C nanotubes. Reproduced with permission [98]. Copyright 2016, Elsevier Ltd.

pollution-free reactants. However, the preparation of efficient and low-cost catalysts has limited the large-scale implementation of this solution. TMDs nanotubes are considered as a potential catalyst for electrochemical hydrogen precipitation due to their wide range of electrical properties and special structural characteristics. Han *et al.* [66] prepared a $MoS_2$@C nanotube hydrogen evolution catalyst by confining the epitaxial growth of few-layered of curved $MoS_2$ within a tubular mesoporous graphene nanotube framework (Fig. 7a). The $MoS_2$@C nanotubes in the form of arrays exhibited excellent performance in electrocatalytic hydrogen evolution applications due to their unique and beneficial structural characteristics. It only needs a low overpotential of 93 mV to deliver a current density of 10 mA/cm$^2$, exceeding that of other structured 2H-$MoS_2$ catalysts (Fig. 7b). In addition, $MoS_2$@C nanotubes also exhibited much lower overpotentials than commercial Pt/C hydrogen evolution catalysts while comparing at a high current density of 1500 mA/cm$^2$ (Fig. 7c). 1D-TMDs nanotubes have also been extensively studied in energy storage applications.

The method of applying solar energy to battery storage systems has received widespread attention due to its green and sustainable effects. However, in the practical application of air batteries, the relatively slow dynamic reaction process of the air cathode has become an obstacle to further development. TMDs nanotubes with excellent photoelectric performance and chemical stability, have been used to design metal-air batteries with high-efficiency storage capabilities. Liang *et al.* [67] prepared a high-performance photo-assisted metal-air battery based on a 1D domain-limited functional $MoS_2$ nanotubes ($MoS_2$_ONT) (Fig. 7d). As shown in Fig. 7e, $MoS_2$_ONT based photo-assisted Zn−air batteries had a higher power density than conventional $MoS_2$ nanosheet ($MoS_2$_NS). At the same time, $MoS_2$_ONT photo-assisted air batteries exhibited a more stable average discharge platform and higher specific capacity than that of $MoS_2$_NS. (Fig. 7f). Fig. 7g showed the mechanism that $MoS_2$_ONT can significantly enhanced the carrier separation kinetics under light. Compared with $MoS_2$_NS, $MoS_2$_ONT with excellent spatial structure is able to form a special electric field in the field of batteries, which can effectively enhance light absorption and fast electron transfer.

1D (TMDs) nanotubes showed great potential in the preparation of high-performance optoelectronic devices due to their unique electrical and optical properties. Zhao *et al.* [103] used a solvent-free method to prepare $MoS_2$ tubular nanoscrolls with excellent photosensitivity for the study of photodetectors (Fig. 7h). Fig. 7i showed the photocurrent-to-dark current ratio (PDR) of

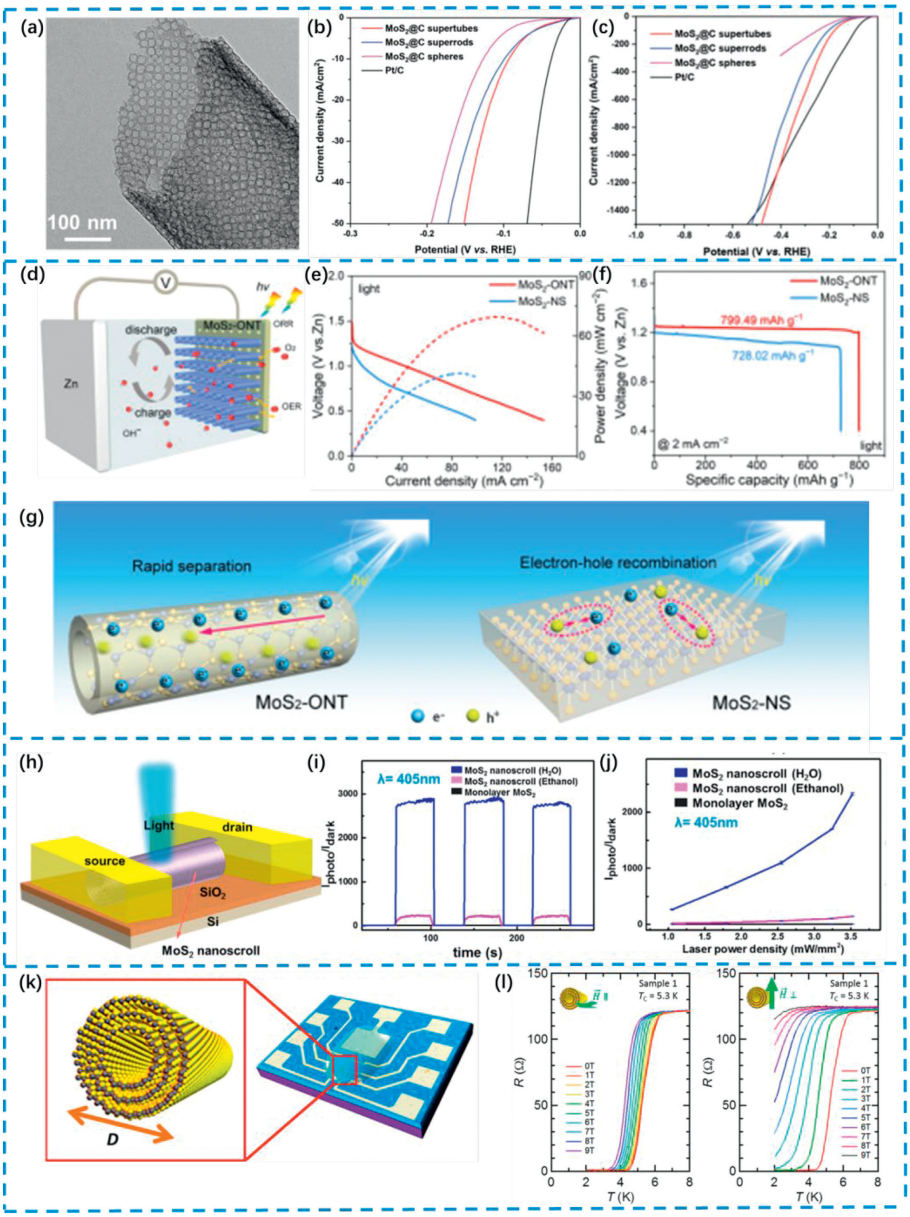


**Fig. 7.** (a) TEM images of tubular graphene frameworks. (b) Polarization curves of various $MoS_2$@C catalysts. (c) Polarization curves at high current densities. Reproduced with permission [66]. Copyright 2023, Wiley-VCH GmbH. (d) Schematic diagram of $MoS_2$_ONT for the preparation of a photo-assisted Zn−air battery. (e) Discharge polarization and power density curves of the photo-assisted Zn−air batteries with $MoS_2$_ONT and $MoS_2$_NS cathodes with light on, respectively. (f) The specific capacity of the Zn–air battery at a current density of 2 mA/cm$^2$ under irradiation. (g) Schematic diagram of the photogenerated electron-hole pairs separation process. Reproduced with permission [67]. Copyright 2023. Wiley-VCH GmbH. (h) Schematic diagram of photoelectric detection device based on $MoS_2$ nanoscrolls. (i) Photocurrent-dark current ratio of molybdenum disulfide nanosheets and NS photodetectors. (j) Under 405 nm laser irradiation, the PDR curves of $MoS_2$ nanosheets, $MoS_2$ nanoscrolls ($H_2O$) and $MoS_2$ nanoscrolls (ethanol) change with the laser power density, respectively. Reproduced with permission [103]. Copyright 2022, American Chemical Society. (k) Schematic of a $WS_2$ nanotube electric-double-layer transistor. (l) Temperature-dependent diagrams of resistance under magnetic fields parallel to and perpendicular to the axis of nanotubes during superconducting transition. Reproduced with permission [104]. Copyright 2024, American Chemical Society.

$MoS_2$ nanoscrolls and single-layer $MoS_2$ nanosheets photodetectors measured under a laser with a wavelength of 405 nm. The PDR of $MoS_2$ nanoscrolls is significantly higher than that of monolayer $MoS_2$ nanosheets, indicating that $MoS_2$ nanoscrolls have excellent photosensitivity. The PDRs of $MoS_2$ nanoscrolls and $MoS_2$ nanosheets as a function of the laser power intensity are shown in Fig. 7j. The PDR of $MoS_2$ nanoscrolls increased significantly with the increase of power intensity, indicating that $MoS_2$ nanoscrolls based photodetectors had better photoresponse performance and higher power dependence.

TMDs nanotubes are considered to be an ideal platform for the study of superconductivity due to their unique size and geometry. Qin *et al.* [104] combined with ionic gating technology to conduct in-depth research on the superconductivity of multi-walled $WS_2$ nanotubes with sizes ranging from tens of nanometers to hundreds of nanometers. Fig. 7k showed an electrical double-layer transistor device of a single $WS_2$ nanotube. After electrochemical $K^+$ intercalation, the $WS_2$ nanotube was transformed into metal and exhibited superconducting properties at low temperatures. Fig. 7l showed the relationship between resistance and temperature during the superconducting phase transition when the magnetic field was parallel and perpendicular to the nanotube axis. Sample 1 exhibited a superconducting transition at the critical temperature $T_c = 5.3$ k, which was defined as half of the normal resis-

tance. Under a parallel magnetic field, nanotubes still exhibited excellent superconductivity even at $T=2$ K and $\mu_0 H=9$ T. However, under perpendicular magnetic field, the superconductivity of nanotubes decreased rapidly. The present results were pivotal in opening up superconductivity in nanotubes and also demonstrated the great potential that existed in TMDs nanotubes for the study of superconductivity. 1D-TMDs nanotubes have demonstrated excellent physical and chemical properties in a variety of applications.

## 5. Conclusion and outlooks

Two-dimensional (2D) TMDs materials have become a hot research topic in recent years due to their unique physical and chemical properties. In addition to extensive research on the optical and electronic properties of 2D materials, their applications in developing renewable energy sources and storage have also been extensively investigated. In this context, 1D TMDs nanotubes transformed from 2D materials are considered as ideal materials with great potential for applications in optoelectronic devices, catalysis, energy storage and superconductivity due to their enhanced intrinsic photovoltaic effect, superconductivity, high strength, flexibility and other novel properties. However, the preparation of nanotubes is still the biggest challenge currently faced. In order to fully understand the differences between the current nanotube preparation methods, it is necessary to summarize the various nanotube preparation methods.

In this paper, we review various preparation methods for high-quality 1D-TMDs nanotubes. We categorize the preparation methods of 1D-TMDs nanotubes into bottom-up and top-down. Bottom-up preparation methods include AAO template method, 1D material template method and metal-catalyzed method. The AAO template has high stability, uniformity and removability, and can be used to prepare nanotubes with controllable morphology. However, the high energy consumption in the process of making templates leads to high costs, which limits its scale-up application. 1D material template method is simple and low cost, but the template cannot be etched and can only be presented as a composite structure. The metal-catalyzed method can precisely regulate the growth process of nanotubes by adjusting the temperature to prepare the chiral angle controllable nanotubes. However, the complex preparation process and high temperature make it limited in the application process. The top-down preparation methods include nanosheet self-curling method and nanosheet stacking method. The controllable multi-walled nanotubes can be prepared by the nanosheet self-curling method. The operation is simple and the cost is low, which is suitable for scale-up application. The nanosheet stacking method can maximize the advantages of 2D nanosheets while generating some new properties of the prepared nanotubes, but the pore size of the nanotubes cannot be accurately controlled. Therefore, further research on the synthesis of high-quality nanotubes is still necessary. With the assistance of artificial intelligence (AI), the synthesis methods of high-quality nanotubes have been further developed. By establishing the model and algorithm, the synthesis process of nanotubes can be simulated to optimize morphology and structure of nanotubes. Therefore, the development process of high-quality nanotubes can be effectively accelerated through the combination of machine learning and computational chemistry methods. In fact, through molecular dynamics (MD) simulation, the morphology, mechanical properties and electronic structures of nanotubes can be further investigated at the nanoscale, effectively reducing the experimental cost and improving the experimental efficiency. In addition, advanced *in situ* characterization technology is indispensable for the preparation of nanotubes. By utilizing *in situ* SEM, XRD and HRTEM, we can have a clearer understanding of the structural evolution of nanotubes and the electron transfer process. The application of these advanced *in situ* characterization techniques will further improve the understanding of the structure and properties of various other TMDs nanotubes.

In conclusion, although TMDs nanotubes have been widely studied and applied, there are still some challenges for their preparation. Researchers in various fields are actively communicating and cooperative to try to solve these challenges. We believe that simple, controllable and low-cost nanotube preparation methods will strongly promote the development of high-performance optoelectronic devices, catalysts and energy storage fields.

## Declaration of competing interest

The authors declare that they have no known competing financial interests or personal relationships that could have appeared to influence the work reported in this paper.

## CRediT authorship contribution statement

**Fengshun Wang:** Writing – original draft. **Huachao Ji:** Investigation, Resources. **Zefei Wu:** Investigation. **Kang Chen:** Software. **Wenqi Gao:** Investigation, Resources. **Chen Wang:** Investigation, Software. **Longlu Wang:** Resources, Supervision, Writing – review & editing. **Jianmei Chen:** Formal analysis, Investigation. **Dafeng Yan:** Funding acquisition, Supervision, Writing – review & editing.

## Acknowledgment

This work was financially supported by the National Natural Science Foundation of China (No. 22202065).

## References

[1] R. Yang, Y. Fan, Y. Zhang, et al., Angew. Chem. Int. Ed. 62 (2023) 1433–7851.
[2] A. Albu-Yaron, S.S. Sinha, R. Tenne, ACS Energy Lett. 5 (2020) 1498–1511.
[3] Y. Huang, W. Quan, H. Yao, et al., Inorg. Chem. Front. 10 (2023) 352–369.
[4] L. Li, P. Wang, Q. Shao, et al., Chem. Soc. Rev. 49 (2020) 3072–3106.
[5] C. Martella, C. Mennucci, A. Lamperti, et al., Adv. Mater. 30 (2018) 9.
[6] W. Zhao, C. Cui, Y. Xu, et al., Adv. Mater. 35 (2023) 2301593.
[7] W. Yao, C. Hu, Y. Zhang, et al., Ind. Eng. Chem. Res. 1 (2023) 106–116.
[8] Z. Xia, S. Guo, Chem. Soc. Rev. 48 (2019) 3265–3278.
[9] Q.M. Liang, X. Wang, X.W. Wan, et al., Nano Res. 16 (2023) 8655–8669.
[10] R.P. Jansonius, P.A. Schauer, D.J. Dvorak, et al., Angew. Chem. Int. Ed. 59 (2020) 12192–12198.
[11] B. Willocq, V. Lemaur, M. El Garah, et al., Chem. Comm. 52 (2016) 7608–7611.
[12] L. Wang, X. Liu, Q. Zhang, et al., Nano Energy 61 (2019) 194–200.
[13] Y. Dong, Z. Ma, I. Lopez, et al., Mater. Today Energy 41 (2024) 101528.
[14] D. Rhee, Y.A.L. Lee, T.W. Odom, ACS Nano 17 (2023) 6781–6788.
[15] M. Luo, S. Guo, Nat. Rev. Mater. 2 (2017) 17059.
[16] H. Du, Q. Liu, N. Cheng, et al., J. Mater. Chem. A 2 (2014) 14812–14816.
[17] F. Wang, L. Xie, N. Sun, et al., Nano-Micro Lett. 16 (2023) 32.
[18] Z. Jiang, W. Zhou, A. Hong, et al., ACS Energy Lett. 4 (2019) 2830–2835.
[19] Y. Yuan, J. Pan, W. Yin, et al., Chin. Chem. Lett. 3 (2024) 108724.
[20] C. Chang, L. Wang, L. Xie, et al., Nano Res. 15 (2022) 8613–8635.
[21] G. Han, X. Zhang, W. Liu, et al., Nat. Commun. 12 (2021) 6335.
[22] K. Jiang, M. Luo, Z. Liu, et al., Nat. Commun. 12 (2021) 1687.
[23] K. Chen, J. Pan, W. Yin, et al., Chin. Chem. Lett. 34 (2023) 108226.
[24] J. Li, W. Yin, J. Pan, et al., Nano Res. 16 (2023) 8638–8654.
[25] C. Sun, L. Wang, W. Zhao, et al., Adv. Funct. Mater. 32 (2022) 2206163.
[26] D. Liu, X. Li, S. Chen, et al., Nat. Energy 4 (2019) 512–518.
[27] L. Xie, L. Wang, W. Zhao, et al., Nat. Commun. 12 (2021) 5070.
[28] J. Yang, Z. Wang, C.X. Huang, et al., Angew. Chem. Int. Ed. 60 (2021) 22722–22728.
[29] P. Fan, Y. He, J. Pan, et al., Chin. Chem. Lett. 35 (2024) 108513.
[30] M. Liu, H. Li, S. Liu, et al., Nano Res. 15 (2022) 5946–5952.
[31] L. Zhang, Z. Shi, Y. Lin, et al., Front. Chem. 10 (2022) 866415.
[32] W. Zhang, H. Hao, Y. Lee, et al., Adv. Funct. Mater. 32 (2022) 2111529.
[33] J. Li, J. Pan, W. Yin, et al., Chin. Chem. Lett. 34 (2023) 108049.
[34] M. Li, L. Wang, X. Zhang, et al., Chin. Chem. Lett. 34 (2023) 107775.
[35] S. Wang, L. Wang, L. Xie, et al., Nano Res. 15 (2022) 4996–5003.
[36] G. Zhou, Y. Shan, L. Wang, et al., Nat. Commun. 10 (2019) 399.
[37] F.L. Deepak, M. Jose-Yacaman, Isr. J. Chem. 50 (2010) 426–438.
[38] S. Aftab, M.Z. Iqbal, Y.S. Rim, Small 19 (2022) 2205418.
[39] B. Zhao, Z. Wan, Y. Liu, et al., Nature 591 (2021) 385–390.
[40] X. Zhou, Z. Jin, J. Zhang, et al., Nanoscale 15 (2023) 2276–2284.
[41] Y. Li, B. Yu, H. Li, et al., Chin. Chem. Lett. 34 (2023) 107874.
[42] W. Yin, Y. Cai, L. Xie, et al., Nano Res. 16 (2022) 4381–4398.

[43] X. Liu, Y. Hou, M. Tang, et al., Chin. Chem. Lett. 34 (2023) 107489.
[44] W. Hu, L. Xie, C. Gu, et al., Coord. Chem. Rev. 506 (2024) 215715.
[45] S. Jiao, M. Kong, Z. Hu, et al., Small 18 (2022) 2105129.
[46] Y. Nakanishi, S. Furusawa, Y. Sato, et al., Adv. Mater. 35 (2023) 2306631.
[47] K. Xu, F. Wang, Z. Wang, et al., ACS Nano 8 (2014) 8468–8476.
[48] D.Y. Hwang, K.H. Choi, D.H. Suh, Nanoscale 10 (2018) 7918–7926.
[49] B. Jia, Q. Yu, Y. Zhao, et al., Adv. Funct. Mater. 28 (2018) 1803409.
[50] Q. Zhou, R. Sun, Y. Ren, et al., Carbon Ener. 5 (2022) 2637–9368.
[51] S. Zhang, W. Wang, F. Hu, et al., Nano-Micro Lett. 12 (2020) 140.
[52] J. Wu, X. Ge, Z. Li, et al., Electrochim. Acta 252 (2017) 101–108.
[53] J. Li, L.X. Chen, X.X. Liu, et al., ACS Appl. Nano Mater. 4 (2021) 14086–14093.
[54] N. Cheng, N. Wang, L. Ren, et al., Carbon 163 (2020) 178–185.
[55] J. Chen, J. Liu, J.-Q. Xie, et al., Nano Energy 56 (2019) 225–233.
[56] C. Sun, M. Liu, L. Wang, et al., Chin. Chem. Lett. 33 (2022) 1779–1797.
[57] Z. Liu, X. Zhang, B. Wang, et al., J. Phys. Chem. C 122 (2018) 12589–12597.
[58] D. Yan, C. Xia, W. Zhang, et al., Adv. Energy Mater. 62 (2022) e202214333.
[59] W. Yin, L. Yuan, H. Huang, et al., Chin. Chem. Lett. 35 (2024) 108351.
[60] N. Abid, A.M. Khan, S. Shujait, et al., Adv. Colloid Interface Sci. 300 (2022) 102597.
[61] Y. Gao, X. Hua, W. Jiang, et al., Angew. Chem. Int. Ed. 61 (2022) e202210924.
[62] Z. Yin, L. Xie, W. Yin, et al., Chin. Chem. Lett. 35 (2023) e202210924.
[63] W. Zhao, B. Jin, L. Wang, et al., Chin. Chem. Lett. 33 (2022) 557–561.
[64] L. Liu, W. Xiong, L. Cui, et al., Angew. Chem. Int. Ed. 59 (2020) 15953–15957.
[65] C.L. Huang, X.F. Chuah, C.T. Hsieh, et al., ACS Appl. Mater. Interfaces 11 (2019) 24096–24106.
[66] W. Han, J. Ning, Y. Long, et al., Adv. Ener. Mater. 13 (2023) 2300145.
[67] S. Liang, L.J. Zheng, L.N. Song, et al., Adv. Mater. 36 (2023) 2307790.
[68] S. Zhao, C. Yang, Z. Zhu, et al., NPJ Comput. Mater. 9 (2023) 92.
[69] Y. Jiang, H. Xiong, T. Ying, et al., Nat. Commun. 15 (2024) 475.
[70] M. Luo, Y. Sun, X. Zhang, et al., Adv. Mater. 30 (2018) 1705515.
[71] Y. Zhang, S.J. Park, J. Mater. Chem. A 6 (2018) 20304–20312.
[72] L. Bu, S. Guo, X. Zhang, et al., Nat. Commun. 7 (2016) 11850.
[73] L. Bu, J. Ding, S. Guo, et al., Adv. Mater. 27 (2015) 7204–7212.
[74] S. Gao, Y. He, H. Li, et al., Energy Stor. Mater. 65 (2024) 103170.
[75] Y. Wei, W. He, P. Sun, et al., Appl. Surf. Sci. 476 (2019) 966–971.
[76] Q. An, W. Xiong, F. Hu, et al., Nat. Mater. 23 (2024) 347–355.
[77] P.X. Gao, Y. Ding, W. Mai, et al., Science 309 (2005) 1700–1704.
[78] P. Cao, J. Wu, Langmuir 37 (2021) 4971–4983.
[79] J.P. Oviedo, S. KC, N. Lu, et al., ACS Nano 9 (2014) 1543–1551.
[80] J. Wu, H. Gong, Z. Zhang, et al., Appl. Mater. Today 15 (2019) 34–42.
[81] D.Y. Hwang, K.H. Choi, J.E. Park, et al., Phys. Chem. Chem. Phys. 19 (2017) 18356–18365.
[82] R. Ghosh, M. Singh, L.W. Chang, et al., ACS Nano 16 (2022) 5743–5751.
[83] J. Liu, Y. Liu, D. Xu, et al., Appl. Catal. B 241 (2019) 89–94.
[84] Z. Jiang, W. Zhou, C. Hu, et al., Adv. Mater. 35 (2023) 2300505.
[85] M. Kaneda, W. Zhang, Z. Liu, et al., ACS Nano 18 (2024) 2772–2781.
[86] S. Zhou, W. Ma, U. Anjum, et al., Nat. Commu. 14 (2023) 5872.
[87] B. Zhou, J. Zhou, L. Wang, et al., Nat. Synth. 3 (2023) 67–75.
[88] L. Wang, F. Zhang, N. Sun, et al., Chem. Eng. J. 474 (2023) 145792.
[89] K. Wang, Z. Hu, P. Yu, et al., Nano-Micro Lett. 16 (2023) 5.
[90] E. Vargo, L. Ma, H. Li, et al., Nature 623 (2023) 724–731.
[91] X. Qiao, X. Yin, L. Wen, et al., Chem 8 (2022) 3241–3251.
[92] S. Lin, B. Wu, Q. Li, et al., Sci. China Mater. 66 (2023) 4669–4679.
[93] T. Liang, A. Wang, D. Ma, et al., Nanoscale 14 (2022) 17841–17861.
[94] J. Li, Z. Pang, C. Gao, et al., Adv. Funct. Mater. 34 (2023) 2306997.
[95] Z. Lai, Y. Chen, C. Tan, et al., Chem 1 (2016) 59–77.
[96] B. Gao, Y. Zhao, X. Du, et al., Adv. Funct. Mater. 33 (2023) 2214085.
[97] D. Bai, Y. Nie, J. Shang, et al., Nano Lett. 23 (2023) 10922–10929.
[98] Z.T. Shi, W. Kang, J. Xu, et al., Nano Energy 22 (2016) 27–37.
[99] W. Deng, C. You, X. Chen, et al., Small 15 (2019) 1901544.
[100] D. Yan, C. Mebrahtu, S. Wang, et al., Angew. Chem. Int. Ed. 16 (2023) e202214333.
[101] L. Liu, Y. Xiao, X. Guo, et al., EES Catal. 2 (2024) 411–447.
[102] J. Chen, Y. Tang, S. Wang, et al., Chin. Chem. Lett. 33 (2022) 1468–1474.
[103] Y. Zhao, H. You, X. Li, et al., ACS Appl. Mater. Interfaces 14 (2022) 9515–9524.
[104] F. Qin, T. Ideue, W. Shi, et al., Nano Lett. 18 (2018) 6789–6794.